2022-02

Magnetic, optical and phase transformation properties of Fe and Co doped VO2(A) nanobelts

Saeidi, SS

10.1016/j.jssc.2021.122729
Journal of Solid State Chemistry
Elsevier BV

Investigation of magnetic, optical and phase transformation properties of VO_2(A) nanobelts influenced by Fe and Co as dopants

Seyedeh Shadi Saeidi[a1], Behrooz Vaseghi[a2], Ghasem Rezaei[a3], Habibollah Khajehsharifi[b4] and David Jenkins[c]

[a] *Department of Physics, College of Sciences, Yasouj University, Yasouj,* 75918-74934, *Iran*

[b] *Department of Chemistry, College of Sciences, Yasouj University, Yasouj,* 75918-74934, *Iran.*

[c] *Wolfson Nanomaterials & Devices Laboratory, School of Computing, Electronics and Mathematics, Plymouth University, Deavon,* PL4 8AA, *UK*

Abstract

In this work, the effects of Fe and Co dopants on the structure, morphology, optical band gap and magnetic properties of VO_2(A) nanobelts with rectangular cross-sections are studied. Our samples have been synthesized by the hydrothermal method and investigated by XRD, FE-SEM, DRS and VSM analysis, respectively. Our optimized synthesis method leads to new structural and physical properties of the samples. The XRD results show our synthesis method could promote the formation of VO_2(B) rather than usual VO_2(A) and cause a transition in VO_2 crystal structure from tetragonal to monoclinic. Furthermore, expanding the lattice of VO_2 by dopants indicates successful substitution of Fe^{3+} and Co^{2+} into the lattice sites of V^{4+}. Optical studies using DRS show dopants can change the optical band gap from 1.13 eV to 1.27 eV. Magnetic measurements using VSM analysis indicate a superparamagnetic behavior for all samples at room temperature.

Keywords: VO_2(A), Hydrothermal synthesis, Phase transformation,

[1] saeidi.sh@gmail.com

[2] Corresponding author. E-Mail: vaseghi@mail.yu.ac.ir

[3] Corresponding author. E-Mail: grezaei@yu.ac.ir.

[4] haka@yu.ac.ir

Optical band gap, Magnetic properties

1. Introduction

During the last few decades, scientists have extensively studied physical properties of transition metal oxide nanostructures and their applications in optical, electronic and magnetic devices [1, 2]. Vanadium is one of the most interesting and important transition metals with various oxidation valence from V^{2+} to V^{5+}, due to partially filled $3d$ shell [3, 4]. These different multivalent oxides result in a variety of VO_2 polymorphs such as monoclinic VO_2(M), rutile VO_2(R), tetragonal VO_2(A), monoclinic VO_2(B), monoclinic VO_2(D), paramontroseite VO_2(P) [5, 6]. It is well known that two series of states can be introduced for vanadium oxides: Magnéli phases (V_nO_{2n-1}) with V^{3+} and V^{4+} ions, and Weysely phases ($V_{2n}O_{5n-2}$) with V^{4+} and V^{5+} ions [7]. Some of these structures are mainly stable and others are metastable. Among various vanadium structures, V_2O_5 with V^{5+} oxidation state is the most stable one and has been used as a precursor in our synthesis. In particular, the first four polymorph phases of VO_2 have attracted a great interest owing to their unique properties and applications. Among them, VO_2(A) has been synthesized for the first time by Theobald [8]. According to his reports, VO_2(A) crystal structure had a tetragonal symmetry without any information about its space group. Few decades later, Oka et al. [9] and then Yao et al. [10] attributed the space group $P42/ncm(138)$ to VO_2(A) [5, 11, 12]. It has been found that an intermediate phase VO_2(A) occurs through a thermal transition between VO_2(B) with the monoclinic and VO_2(R) with the tetragonal-rutile structure. It means by changing the synthesis temperature, a transformation from VO_2(B) to VO_2(A) and then to VO_2(M/R) happens [13]. There are several methods for preparing VO_2(A) such as sol-gel, hydrothermal synthesis, physical vapor deposition, chemical vapor deposition, pyrolysis processes and so on. Among them, the hydrothermal method has received increasing attention due to its reliable, facile and low-cost nature. However, the synthesis of VO_2(A) is a complicated process, its morphology depends on the precursors significantly [14, 15, 16]. There are few reports on hydrothermal method to synthesize VO_2(A). Among these, the following can be mentioned: Liu et al. [11] used a mixed hydrothermal method and investigated phase-transition and thermochromic properties of VO_2(A) long nanorods. M. Li et al. [17] reported hydrothermal synthesized

ultra-long VO_2(A) nanobelts and studied their electrical transport and field-emission properties. Ji et al. [12, 18] synthesized VO_2(A) by controlling on hydrothermal pressure and investigated dopant effect on VO_2(A) nanorods. Zhang et al. [19] studied optical and transition properties of VO_2(A) and Dai et al. [20] prepared nanobelts, nanorods and nanowires by one-step hydrothermal method and studied their electrochemical properties for using them as a cathode in Li-ion batteries. Several other researchers have reported synthesizing VO_2(A) by this method but due to the complexity of production, researches on VO_2(A) are still limited than the other VO_2 polymorphs and thus its optical and magnetic properties have not been studied widely [21]. However, most investigations of VO_2 have been done on the metal-to-insulator phase transition (MIT) which leads to sharp changes in electrical and thermal properties, the main part of this work is devoted to studying the effects of common magnetic transition metal dopants such as Fe and Co on VO_2(A). To this aim, at first, we have synthesized VO_2(A) with the optimal hydrothermal procedure. Next, using this procedure $V_{0.97}Fe_{0.03}O_2$, $V_{0.97}Co_{0.03}O_2$ and $V_{0.94}Fe_{0.03}Co_{0.03}O_2$ are obtained and their magnetic hysteresis, optical band gap and crystalline stability are investigated.

2. Experimental section

2.1. Materials

Vanadium Pentoxide (V_2O_5), oxalic acid dihydrate ($C_2H_2O_4.H_2O$), hydrogen peroxide (H_2O_2, 30wt%), iron(III) nitrate nonahydrate ($Fe(NO_3)_3.9H_2O$), and cobalt(II) nitrate hexahydrate ($Co(NO_3)_2.6H_2O$) were received from Merck Co., Germany. All of the chemical reagents were used without any further purification.

2.2. Synthesis of VO_2(A)

VO_2(A) was synthesized by a one-step hydrothermal method using V_2O_5 as the vanadium source and a reducing agent of oxalic acid. In a typical synthesis, 0.45 g of V_2O_5 and 1.70 g of oxalic acid (1 : 3 in molar ratio) were dispersed in 70 ml of double distilled water under vigorous magnetic stirring at 80 $^{\circ}C$ for 2 hours to form a clear dark blue solution indicating a complete reduction of V^{5+} into V^{4+} [12, 18, 22, 23]. After cooling to room temperature naturally, an appropriate amounts of $Fe(NO_3)_3.9H_2O$ or/and $Co(NO_3)_2.6H_2O$ were added to the prepared solution. Subsequently, the well-mixed precursor was transferred into a 110 mL Teflon-lined-autoclave

and 3 ml of H_2O_2, 30 wt% as a strong oxidizer was added exactly up to 75% of autoclave volume which is responsible as an important factor to achieve the desired phase. Also, Argon gas was used as the purge for 5 minutes and then the autoclave was sealed, heated to 245 $^\circ C$ and kept at that temperature for 24 hours. Then, it was cooled to room temperature in the air. The resulting precipitates were washed and centrifuged three times at 4000 rpm for 15 minutes with double distilled water. Finally, our product was dried at 80 $^\circ C$ for 6 hours and the obtained powder was annealed in 300 $^\circ C$ for 1 hour.

2.3. Characterization

The phase structure of the produced powders was determined using X-Ray Diffractometer (XRD; Bruker D8 Advance, Germany) using Cu K_α radiation ($\lambda = 0.15418\ nm$). The structure and morphology of the products were examined by a field emission scanning electron microscope (FESEM, SIGMA VP, ZEISS, Germany), Energy Dispersive X-ray Spectroscopy (EDS) coupled to the FESEM was used to determine chemical elements and the homogeneity of samples. Furthermore, the spatial distribution of elements in samples were determined using elemental mapping. Vibration Sample Magnetometer (VSM; Kashan, Iran) was used to investigate the magnetic properties of our samples. The optical band gap of samples was measured by using a diffuse reflection spectroscopy (DRS) (Avaspec-2048-TEC, Avantes Co., Netherlands).

3. Results and discussion

3.1. Crystalline structures

The XRD patterns of prepared powders under the same hydrothermal process have been illustrated in Fig. 1. Diffraction peaks in the pattern as shown in Fig. 1a, can be indexed into tetragonal VO_2 since they correspond precisely to the standard JCPDS Card No. $42-0876$ (space group: $P42/ncm(138)$) with lattice parameters $a = b = 8.450\ \mathring{A}$, $c = 7.686\ \mathring{A}$ and $\alpha = \beta = \gamma = 90^\circ$ [24, 25]. Over the drying procedure in which the shape and the size of the particles in the sample are formed, most of them have a chance to orient in preferred crystallographic direction [26]. So, high-intensity peaks in $2\theta = 14.92^\circ$, 29.92° and 45.51° exhibit the preferential crystalline orientation along the [110], [220] and [330] directions, respectively. Consequently, based on the results of the X-ray diffraction spectrum, peaks with strong intensities which aligned in the ($nn0$) family of crystal planes are referred to the

preferred orientation crystal growth of VO_2(A) nanobelt which is synthesized without any additives as dopants and impurities [27].

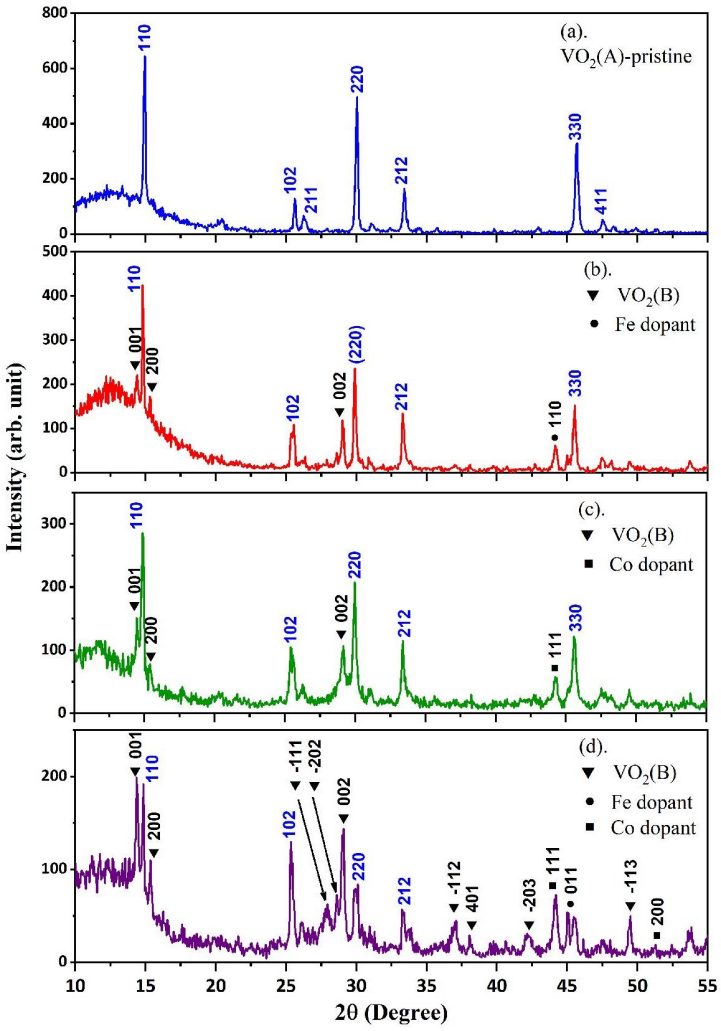

Figure 1: XRD patterns of prepared sample

The other XRD patterns which are related to adding dopants into VO_2(A) have been presented in Figs. 1.b to 1.d. These figures show a slight red shift in all of the diffraction peaks and it seems reasonable to assume Fe and Co dopants lead to expand the lattice of VO_2, because the ionic radius of V^{4+} (0.58 $\AA$, coordination number (CN)= 6) is smaller than that of Fe^{3+} (0.65 $\AA$,

CN = 6) [27, 28] and Co^{2+} (0.75 $\AA$, CN = 6). Fig. 2 represents the shift in (110) plane of doped samples in comparison with the VO_2-pristine sample as the reference peak.

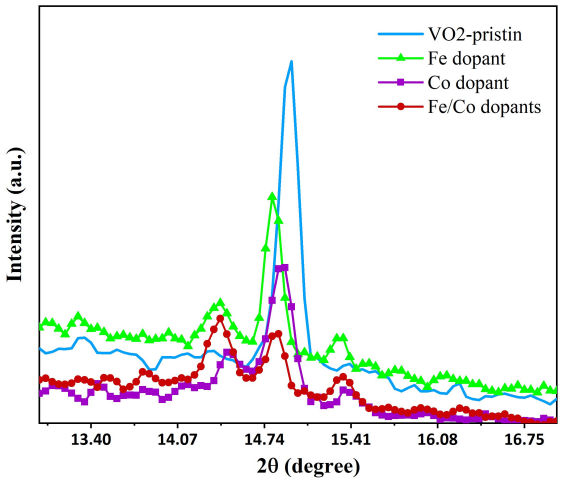

Figure 2: Comparison of (110) peaks in samples

According to the Bragg equation (1) the distance between crystalline planes, d_{hkl}, can be calculated by [29]:

$$2d_{hkl}sin\theta = n\lambda \tag{1}$$

where λ is the X-ray wavelength, θ and n are the angle of incident beam and integer number, respectively. The obtained results indicate that inter-planar distance increases by adding dopants. The calculated results have been shown in Table 1.

Sample	$2\theta(^\circ)$	FWHM $(^\circ)$	d_{110}(Å)
VO_2-pristine	14.92	0.142	2.989
Fe-doped	14.81	0.113	3.013
Co-doped	14.85	0.093	3.003
Fe/Co-doped	14.87	0.090	3.000

Table 1: Crystalline parameters of the XRD patterns for synthesized samples

On the other hand, full width at half maximum (FWHM) value of the highest peak at (110) plane in the doped samples undergoes a decrease of

0.113°, 0.093° and 0.090° for Fe-doped, Co-doped and Fe/Co-doped, respectively, in comparison with 0.142° of VO_2(A). This result that FWHM of VO_2(A) pristine is greater than that of VO_2 with dopants is an evidence that the impurity ions successfully incorporate in the lattice of the VO_2 as substituent [29, 30, 31]. Furthermore, it is found that the reduction in the peaks intensity by adding Co into VO_2(A) is greater than that of Fe-doped, which shows that the Co dopant decreases the crystallinity. On the other hand, our doped synthesized samples promote the VO_2(A) to a second phase, VO_2(B) [25]. Since the main basic units of VO_2 polymorphs are octahedral VO_6 units, so it is worth mentioning that different bond angles between oxygen and vanadium atoms in $V-O-V$ covalent bonds are responsible for various geometry, structural tension and thermodynamic stability. These units in VO_2(A) are the same but there are two different types of VO_6 in VO_2(B) due to the distortion of vanadium atom from the center of octahedral in compared with regular units of VO_2(A). This deviation can make an open and penetrable framework in the structure of VO_2(B). In this regard, by adding additives in samples bond angles of the regular octahedral unit with less electronic repulsion in VO_2(A) change in such a way that they cause a kind of distortion in the octahedral basic unit which increase the structural tension and electronic repulsion and then arise instability in phase structure [25, 32, 33, 34]. Consequently, since VO_2(A) is thermodynamically more stable than VO_2(B) due to its higher formation energy [25, 34], the appearance of VO_2(B) by adding additives in samples reflects the fact that the larger ionic radii of Fe^{3+} and Co^{2+} than that of V^{4+} lead to the change in bond angles and the nucleation of VO_2(B) [35]. Moreover, adding dopants may have an influence on the positions of V atoms and it can be led to the formation a new phase by the appearance of the extra peaks in X-ray patterns which belong to the monoclinic VO_2(B) (JCPDS, No. $81-2392$, $C2/m$) as a second phase [31]. These peaks in Fe-doped sample are sharper than that with Co-doped because the density of Fe in our sample is greater as EDS analysis shows (Fig. 4). In the last XRD diffraction pattern, Co and Fe simultaneously doped in VO_2(A), the number of peaks assigned to VO_2(B) are more than that of the samples with Fe or Co doped lonely. It may be attributed to the increase in inter-planar spacing in VO_2(A) due to adding both dopants at the same time with larger ionic radii than that of V^{4+} and therefore the structure tends to be unstable [15].

3.2. Surface morphology

FESEM images of VO_2(A) with and without additives have been illustrated in Fig. 3(a, b, c and d) at two different magnifications. As can be seen, the crystal morphology of VO_2(A) is nanobelt. These belts have rectangular cross-sections with different widths, lengths and thicknesses in nanometer. It can be found that they have smaller amounts in thicknesses changing approximately from 20 nm to 150 nm and typical widths about $50 - 450$ nm. FESEM images show the morphology does not change with addition of Fe or Co as dopants into this structure and formation of VO_2(B) as the second phase, but it is important to note that some agglomerations form especially by Co/Fe doped and the structure becomes denser.

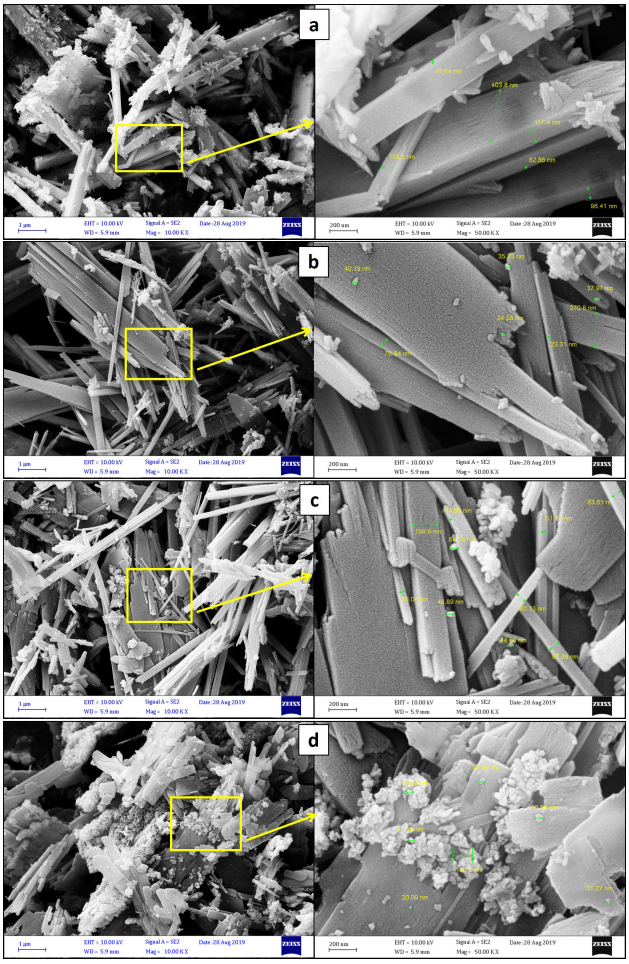

Figure 3: FESEM images of samples with two different magnifications: 1 μm (Left) and 200 nm (Right): (a).VO_2(A) without any additives, (b).Fe-doped, (c).Co-doped, (d).Fe/Co-doped.

The surface analysis by EDS spectrum and elemental mapping have been displayed in Figs. 4 and 5. These analyses indicate that all of the samples consist of V, O and additives with the homogeneous distributions.

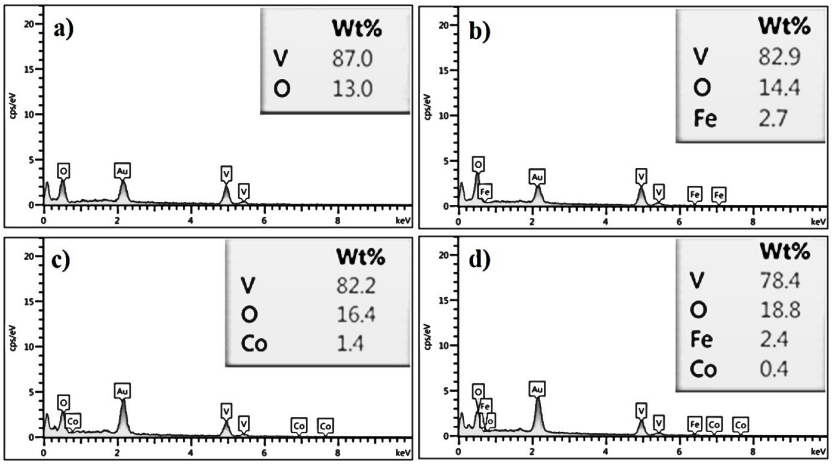

Figure 4: EDS spectrum of: (a).VO_2-pristine, (b).Fe-doped, (c).Co-doped, (d).Fe/Co-doped.

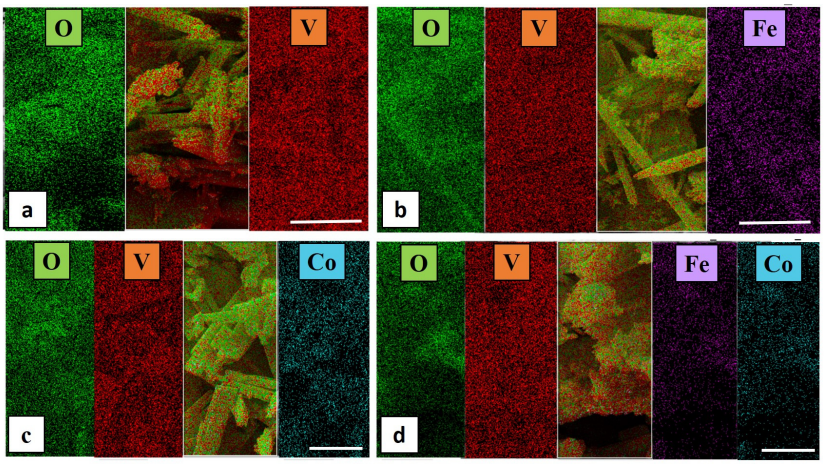

Figure 5: FESEM mapping of:(a).VO_2-pristine, (b).Fe-doped, (c).Co-doped, (d).Fe/Co-doped. (The scale bar is 1 μm)

3.3. Magnetic properties

The magnetic properties of VO_2 with and without dopants have been investigated using vibrating sample magnetometer (VSM) at room temperature. The hysteresis loops of the samples, magnetization (M) against applied magnetic field (H), have been plotted in Fig. 6. The field sweeps from -14 to 14 kOe but still saturation does not happen. It is worth mentioning that

VO_2-pristine has been used as a reference sample to compare with doped samples. Since vanadium is a transition metal with partially filled d orbital, [Ar] $3d^3 4s^2$, so due to the existence of unpaired electrons, VO_2-pristine has a paramagnetic behavior [36]. It can be seen VO_2-pristine saturates in very low magnetization, but adding magnetic transition metals such as Fe and Co can induce a change in magnetization of our samples in which adding Co/Fe simultaneously into VO_2 causes larger magnetization than adding Fe and Co separately. Moreover, all samples indicate a superparamagnetic behavior due to their negligible remanence magnetization and coercivity.

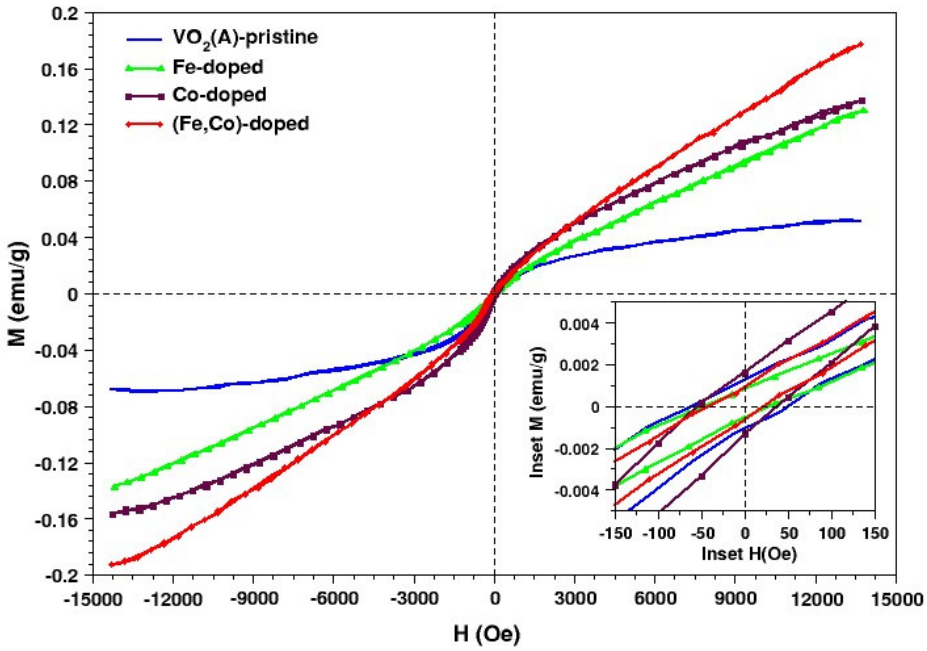

Figure 6: Hysteresis loop of as-prepared samples, indicating magnetization (M) against applied magnetic field (H). (inset: M vs H curve for present samples

All the information about saturated and remanence magnetization and coercivity have been shown in Table 2.

Sample	M_S (emu/g)	H_c (Oe)	M_r (emu/g)
VO_2-pristine	0.05	55.17	0.0012
Fe-doped	0.13	37.55	0.0007
Co-doped	0.14	46.08	0.0015
Fe/Co-doped	0.18	31.71	0.0008

Table 2: Saturated magnetization (M_S), Coercivity (H_c) and remanence (M_r) of synthesized samples

In detail, in transition metal oxides like VO_2 with the octahedral units, $2p$ orbitals of oxygen ligands overlap with metal $3d$ orbitals and cause to form partially covalent bonds. But, t_{2g} states contribute to overlap with p orbitals less than e_g states. Hence, the e_g states are higher in energy. This overlap results in the formation of bonding and antibonding states. The magnetic properties of materials strongly depend on the amounts of splitting between sub-bands near the fermi level, so the more overlap increases the more electronic repulsion and thus the strong splitting happens [37, 38]. In $3d$ magnetic dopants, the amount of the splitting determines the strength of the ferromagnet which means Co is the stronger ferromagnet than Fe. Moreover, adding magnetic dopants causes a broadening in impurity states near the fermi level. It means there are more electrons to hybridize with d-orbitals of impurity. So the number of unpaired electrons in dopant decreases and magnetic moments will be destroyed [38]. As an accepted rule in semiconductors, heavy $3d$ impurities which are started from Cr, retain their uncompensated magnetic moments, although the lighter $3d$ transition metals are nonmagnetic [39]. In spite of the fact that the number of magnetic moments in Co is less than that in Fe, but the residual uncompensated magnetic moments in Co is more. Thus the net magnetization is higher in adding Co [38, 40]. There is a declining trend in coercivity and it may be attributed to decreasing the belt dimensions. But an unusual enhancing is seen in Co-doped sample which may be related to the change in the size of the belts [40].

3.4. Band gap analysis

The other analysis is diffuse reflection spectroscopy (DRS) which measures the optical band gap, E_g, of materials. The optical band gap is an important quantity in determining the material used for optoelectronic devices and photocatalyst depending upon that the material is an insulator,

semiconductor or metal. The diffused reflectance spectrum of the sample powders is analyzed by the Kubelka-Munk theory which is formulated in Eq. (2) [41]:

$$F(R) = \frac{\alpha}{S} = \frac{(1-R)^2}{2R} \tag{2}$$

where $F(R)$ is the Kubelka-Munk function, R, α and S are the reflectance, absorption coefficient and scattering factor, respectively. Moreover, due to an ignorance dependency between scattering factor and wavelength, S can be considered as a constant and as a result, $F(R)$ is proportional to α [42, 43]. Thus, the optical band gap is determined by plotting absorption coefficient against photon energy known as Tauc plot and extrapolating of a straight line to photon energy axis in plot. According to the following relation (Tauc plot) [44, 45, 46]:

$$\alpha h\nu = k(h\nu - E_g)^{n/2} \tag{3}$$

where α is the absorption coefficient, h and k are respectively the Planck's and an energy-independent constant. Determining the exponent n in Eq. (3) depends on the four types of transitions: direct- and indirect- with $n = 2$ and $1/2$ for allowed, $2/3$ and $1/3$ for forbidden transitions, respectively [41, 43]. The direct band gap, $n = 2$, is found to be the right choice for a straight line near the absorption edge [47, 48]. It is important to notice that by adding dopants into VO_2, the optical band gap changes. Fig. 7 shows that the calculated values for VO_2-pristine, Fe-doped, Co-doped and Fe/Co-doped are 1.20, 1.13, 1.17 and 1.27 eV, respectively. To our knowledge this values for doped VO_2(A) have not been reported yet.

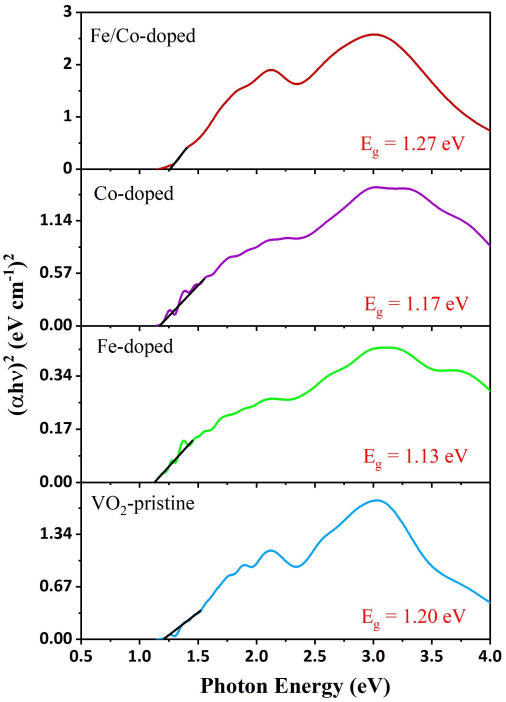

Figure 7: Band gap of VO_2-pristine and VO_2 with dopants.

Based on the molecular orbital diagram of VO_2(A) (see Fig.8) which has been depicted by Zhang et al. [34], the $3d$ orbitals of vanadium are split into two levels due to the octahedral crystal field: higher e_g and lower t_{2g} states in energy. Furthermore, hybridization occurs between V-$3d$ and O-$2p$ orbitals in such a way that e_g- and p-orbitals make σ bonding and anti-bonding levels with strong splitting. Besides, t_{2g} orbitals hybrid with O-p states and make π and π^* interactions. On the other hand, electronic repulsion due to the distortion of octahedral units in VO_2(A), splits $d_{||}$ bands into two parts in which fully occupied band places under the fermi level and upper than the π states, whereas the unoccupied part pushes down the empty π^* band near the fermi-level, as illustrated in Fig. 8. As a result of this splitting, a band gap is opened between $d_{||}$ band bellow the fermi level and π^*. In comparison with VO_2(A)-pristine, decreasing band gap in Fe-doped and Co-doped samples is owing to the introducing intermediate electronic states. They originate from $3d$ electrons of dopants and their interaction with the host orbitals which may increase their overlap, broaden the impurity levels and push some of

sub-bands near the fermi energy like as a donor or acceptor. So, all of these processes decrease the band gap. On the other hand, due to adding Fe/Co-doped, instability of the structure increases by the appearance of VO_2(B) which has lower symmetry and higher distortion in VO_6 units than VO_2(A). The latter mentioned reason shifts the σ and π bonding; so it can cause the strong splitting and the bigger band gap for Fe/Co-doped [34, 44, 45, 49].

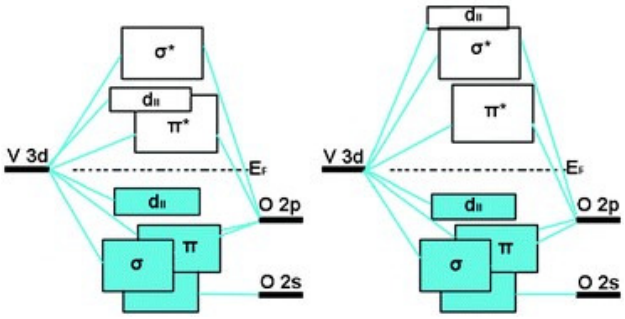

Figure 8: Electronic states of two polymorphs of VO_2 based on Molecular orbital diagram taken from Zhang et al. work [34]: VO_2(A) (left) and VO_2(B) (right)

Also, the interesting and important phenomena of optical absorption reduction and increment by changing dopants is presented in Fig. 9. A glance at this figure reveals that due to the band gap modification with dopants, absorption in visible region increases for Fe/Co-doped and decreases for Co- and Fe-doped samples comparing with the VO_2-pristine. To our knowledge, band gap and thus absorption variation for doped VO_2(A) have not been reported yet.

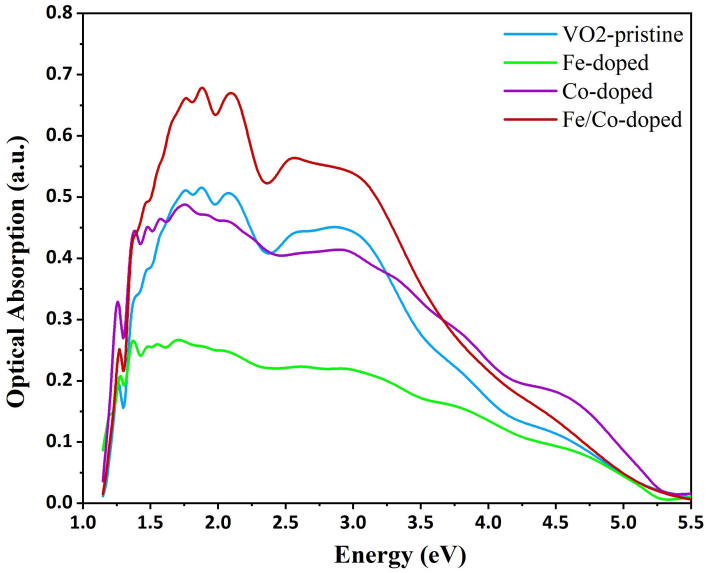

Figure 9: Optical absorption spectrum with respect to the incident photon energy for different atomic dopants.

4. Conclusions

In summary, the one-step hydrothermal method was successfully used to synthesis of VO_2(A) and then prepared samples were characterized by structural, optical and magnetic properties. XRD results reveal the fact that Fe, Co, and their co-dopant can promote the formation of VO_2(B) as a second phase and expanding lattice is in evidence that substitution of impurities into the host material has been effective. Based on the VSM results, our samples except VO_2-pristine exhibit superparamagnetic behavior specifically and residual uncompensated magnetic moments of dopants lead to an increase in magnetization. In addition depending on different dopants, optical band gap changes correspond to the IR region of electromagnetic radiation and the samples are recognized to be a semiconductor.

[1] T. Guo, M.S. Yao, Y.H. Lin, C.W. Nan, A comprehensive review on synthesis methods for transition-metal oxide nanostructures, J. CrystEngComm 17 (2015) 3551-3585. https://doi.org/10.1039/C5CE00034C

[2] G.Y. Song, Ch. Oh, S. Sinha, J. Son, and J. Heo, Facile phase control of multi-valent vanadium oxide thin films (V_2O_5 and VO_2) by atomic layer

deposition and post-deposition annealing, J. ACS Appl Mater Inter. 9 (2017) 23909-23917. https://doi.org/10.1021/acsami.7b03398

[3] S. Loquai, Durable thermochromic VO_2 films deposited by HIPIMS, [PhD thesis]. Canada: École Polytechnique de Montréal; (2017).

[4] S.R. Popuri, M. Miclau, A. Artemenko, C. Labrugere, A. Villesuzanne, M. Pollet, Rapid Hydrothermal Synthesis of VO_2(B) and Its Conversion to Thermochromic $VO_2(M1)$, J. Inorg. Chem. 52 (2013) 4780-4785. https://doi.org/10.1021/ic301201k.

[5] S.R. Popuri, A. Artemenko, C. Labrugère, M. Miclau, A. Villesuzanne, M. Pollet, VO_2(A): Reinvestigation of crystal structure, phase transition and crystal growth mechanisms, J. Solid State Chem. 213 (2014) 79-86. https://doi.org/10.1016/j.jssc.2014.01.037.

[6] Y. Zhang, VO_2(B) conversion to VO_2(A) and VO_2(M) and their oxidation resistance and optical switching properties, J. Mater. Sci.-Poland 34 (2016) 169-176. https://doi.org/10.1515/msp-2016-0023.

[7] N. Bahlawane, D. Lenoble, Vanadium oxide compounds: structure, properties, and growth from the gas phase, J. Chem. Vap. Depos. 20 (2014) 299-311. https://doi.org/10.1002/cvde.201400057.

[8] F. Theobald, J. Less, Étude hydrothermale du système $VO_2 - VO_{2,5} - H2O$, J. the Less Common Met. 53 (1977) 55–71. https://doi.org/10.1016/0022-5088(77)90157-6.

[9] Y. Oka, T. Yao, N. Yamamoto, Powder X-ray crystal structure of VO_2(A), J. Solid State Chem. 86 (1990) 116–124. https://doi.org/10.1016/0022-4596(90)90121-D.

[10] T. Yao, Y. Oka, N. Yamamoto, A structural study of the high-temperature phase of VO_2(A), J. Solid State Chem. 112 (1994) 196–198. https://doi.org/10.1006/jssc.1994.1287.

[11] P. Liu, K. Zhu, Y. Gao, Q. Wu, J. Liu, J. Qiu, Q. Gu, H. Zheng, Ultra-long VO_2(A) nanorods using the high-temperature mixing method under hydrothermal conditions- synthesis, evolution and thermochromic properties, J. CrystEngComm. 15 (2013) 2753-2760. https://doi.org/10.1039/C3CE27085H.

[12] S. Ji, F. Zhang, P. Jin, Selective formation of VO_2(A) or VO_2(R) polymorph by controlling the hydrothermal pressure, J. Solid State Chem. 184 (2011) 2285-2292. https://doi.org/10.1016/j.jssc.2011.06.029.

[13] W. Zhang, L. Shi, K. Tang, Y. Yu, A Facile Fabrication of VO_2(A) Micro-nanostructures with Controlled Shape and Its Electrochemical Behavior in Lithium Ion Batteries, J. Chem. Lett. 41 (2012) 104-106. http://doi.org/10.1246/cl.2012.104.

[14] Y. Zhang, J. Zhang, X. Zhang, C. Huang, Y. Zhong, Y. Deng, The additives W, Mo, Sn and Fe for promoting the for mation of VO_2(M) and its optical switching properties, J. Mater. Lett. 92 (2013) 61–64. https://doi.org/10.1016/j.matlet.2012.10.054.

[15] W. Li, S. Ji, Y. Li, A. Huang, H. Luoad, P. Jin, Synthesis of VO_2 nanoparticles by a hydrothermal assisted homogeneous precipitation approach for thermochromic applications, J. RSC Adv. 4 (2014) 13026-13033. https://doi.org/10.1039/C3RA47666A.

[16] C. Leroux, G. Nihoul, G.V. Tendeloo, From VO_2(B) to VO_2(R): Theoretical structures of VO_2 polymorphs and in situ electron microscopy, J. Phys. Rev. B 57 (1998) 5111-5121. https://doi.org/10.1103/PhysRevB.57.5111.

[17] M. Li, F. Kong, L. Li, Y. Zhang, L. Chen, W. Yan, G. Li, Synthesis, field-emission and electric properties of metastable phase VO_2(A) ultra-high nanobelts, J. Dalton T. 40 (2011) 10961-10965. http://doi.org/10.1039/c1dt10941c.

[18] S. Ji, Y. Zhao, F. Zhang, P. Jin, synthesis and phase transition behavior of W-doped VO_2(A) nanorods, J. Ceram. Soc. JAPAN 118 (2010) 867-871. http://doi.org/10.2109/jcersj2.118.867.

[19] Y. zhong, Y. zhang, X. Liu, X. Liu, C. Huang, H. Li, Synthesis of VO_2(A) Nanostructures by a Hydrothermal Method and Their Transition to VO_2(M), J. Adv. Mater. 295-297 (2011) 368-372. https://doi.org/10.4028/www.scientific.net/AMR.295-297.368

[20] L. Dai, Y. Gao, C. Cao, Z. Chen, H. Luo, M. Kanehir, J. Jin, Y. Liu, VO_2(A) nanostructures with controllable feature sizes

and giant aspect ratios: one-step hydrothermal synthesis and lithium-ion battery performance, J. RSC Adv. 2 (2012) 5265–5270. https://doi.org/10.1039/C2RA20587D.

[21] S. Lee, I.N. Ivanov, J.K. Keum, H.N. Lee, Epitaxial stabilization and phase instability of VO_2 polymorphs, J. Sci. Rep. 6 (2016) 19621-19628. https://doi.org/10.1038/srep19621.

[22] A.C.S. Figueiredo, Growth of Vanadium Dioxide (VO_2) Nanostructures by Controlling the Hydrothermal Synthesis Parameters, [PhD thesis]. Portugal: Universidade Nova de Lisboa; (2016).

[23] M.J. Powell, VO_2 Thin Films and Nanoparticles, from Chemical Hydrothermal Synthesis, for Energy Efficient Applications, [PhD Thesis]. United Kingdom: University College London; (2015).

[24] Y. Zhang, M. Fan, F. Niu, Y. Zhong, C. Huang, X. Liu, B. Wang, H. Li, Hydrothermal synthesis of VO_2(A) nanobelts and their phase transition and optical switching properties, J. Micro Nano Lett. 6 (2011) 888 – 891. http://doi.org.10.1049/mnl.2011.0463.

[25] S. Liang, Q. Shi, H. Zhu, B. Peng, W. Huang, One-Step Hydrothermal Synthesis of W-Doped VO_2(M) Nanorods with a Tunable Phase-Transition Temperature for Infrared Smart Windows, J. ACS Omega 1 (2016) 1139–1148. https://doi.org/10.1021/acsomega.6b00221.

[26] C.F. Holder, R.E. Schaak, Tutorial on Powder X-ray Diffraction for Characterizing Nanoscale Materials, J. ACS Nano. 13 (2019) 7359-7365. https://doi.org/10.1021/acsnano.9b05157.

[27] R. Zhang, H.B. Jin, D. Guo, J. Zhang, Z. Zhao, Y. Zhao, J.B. Li, The role of Fe dopants in phase stability and electric switching properties of Fe-doped VO_2, J. Ceram. Int. 42 (2016) 18764-18770. https://doi.org/10.1016/j.ceramint.2016.09.017.

[28] R.D. Shannon, C.T. Prewitt, Effective Ionic Radii in Oxides and Fluorides, J. Acta Crystallogr B 25 (1969) 925-946. https://doi.org/10.1107/S0567740869003220.

[29] W. Zhao, Z. Wei, L. Zhang, X. Wu, X. Wang, J. Jiang, Optical and magnetic properties of Co and Ni co-doped ZnS nanorods prepared by hydrothermal method, J. Alloys Compd. 698 (2017) 754-760. https://doi.org/10.1016/j.jallcom.2016.12.127.

[30] N. Manjula, M. Pugalenthi, V.S. Nagarethinam, K. Usharani, A.R. Balu, effect of doping concentration on the structural morphological optical and electrical properties of Mn-doped CdO thin films, J. Mater Sci-Poland 33 (2015) 774-781. https://doi.org/10.1515/msp-2015-0115.

[31] Q. Li, H. Meng, P. Zhou, Y. Zheng, J. Wang, J. Yu, J.R. Gong, $Zn_{1-x}Cd_xS$ Solid Solutions with Controlled Bandgap and Enhanced Visible-Light Photocatalytic H2-Production Activity, J. ACS Catal. 3 (2013) 882–889. https://doi.org/10.1021/cs4000975.

[32] W. Yu, Sh. Li, C. Huang, Phase evolution and crystal growth of VO_2 nanostructures under hydrothermal reactions, J. RSC Adv. 6 (2016) 7113-7120. https://doi.org/10.1039/C5RA23898F.

[33] C. Wu, F. Feng, J. Feng, J. Dai, J. Yang, Y. Xie, Ultrafast Solid-State Transformation Pathway from New-Phased Goethite VOOH to Paramontroseite VO_2 to Rutile VO_2(R), J. Phys. Chem. C 115 (2011) 791–799. https://doi.org/10.1021/jp109967j.

[34] S. Zhang, B. Shang, J. Yang, W. Yan, S. Wei, Y. Xie, From VO_2(B) to VO_2(A) nanobelts- first hydrothermal transformation, spectroscopic study and first principles calculation, J. Phys. Chem. Chem. Phys. 13 (2011) 15873-15881. https://doi.org/10.1039/C1CP20838A.

[35] M. Kitamura, Strategy for control of crystallization of polymorphs, J. CrystEngComm. 11 (2009) 949–964. https://doi.org/10.1039/B809332F.

[36] A.A. Akande, K.E. Rammutla, T. Moyo, N.S.E. Osman, S.S. Nkosi, C.J. Jafta, B.W. Mwakikunga, Magnetism variations and susceptibility hysteresis at the metal-insulator phase transition temperature of VO_2 in a composite Film containing vanadium and tungsten oxides, J. Magn. Magn. Mater. 375 (2015) 1-9. https://doi.org/10.1016/j.jmmm.2014.08.099.

[37] R. Rückamp, Orbital excitations of transition-metal oxides in optical spectroscopy, [PhD thesis]. Köln: Universität zu Köln; 2006.

[38] J.M.D. Coey, Magnetism and Magnetic Materials, Cambridge University Press, New York, 2010. pp. 144-154.

[39] K.A. Kikoin, V.N. Fleurov, Transition Metal Impurities in Semiconductors−Electronic Structure and Physical Properties, World Scientific Pub Co Inc, Singapore, 1994. pp. 213-220.

[40] N. Srivastava, P.C. Srivastava, Synthesis of NiO Nanowires/Nanorods and Their Magnetic Characteristics, J. Mater. Focus 2 (2013) 421-428. https://doi.org/10.1166/mat.2013.1112.

[41] S.Y. Li, N.R. Mlyuka, D. Primetzhofer, A. Hallén, G. Possnert, G.A. Niklasson, C.G. Granqvist, Bandgap widening in thermochromic Mg-doped VO_2 thin films Quantitative data based on optical absorption, J. Appl. Phys. Lett. 103 (2013) 161907. https://doi.org/10.1063/1.4826444.

[42] R. Köferstein, S.G. Ebbinghaus, Investigations of $BaFe_{0.5}Nb_{0.5}O_3$ nano powders prepared by a low temperature aqueous synthesis and resulting ceramics, J. Eur. Ceram. Soc. 37 (2017) 1509–1516. https://doi.org/10.1016/j.jeurceramsoc.2016.12.014.

[43] R. Köferstein, L. Jäger, S.G. Ebbinghaus, Magnetic and optical investigations on $LaFeO_3$ powders with different particle sizes and corresponding ceramics, J. Solid State Ion. 249–250 (2013) 1–5. https://doi.org/10.1016/j.ssi.2013.07.001.

[44] Y. Yalçın, M. Kılıç, Z. Çınar, Fe^{+3}−doped TiO_2: A combined experimental and computational approach to the evaluation of visible light activity, Appl. Catal. B 99 (2010) 469-477. https://doi.org/10.1016/j.apcatb.2010.05.013.

[45] S. Hu, S.Y. Li, R. Ahuja, C.G. Granqvist, K. Hermansson, G.A. Niklasson, R.H. Scheicher, Optical properties of Mg-doped VO_2 Absorption measurements and hybrid functional calculations, J. Appl. Phys. Lett. 101 (2012) 201902. https://doi.org/10.1063/1.4766167.

[46] J. Zhou, Y. Gao, X. Liu, Z. Chen, L. Dai, C. Cao, H. Luo, M. Kanahira, C. Sunc, L. Yan, Mg-doped VO_2 nanoparticles hydrothermal synthesis, enhanced visible transmittance and decreased metal−insulator transition temperature, J. Phys. Chem. Chem. Phys. 15 (2013) 7505-7511. https://doi.org/10.1039/C3CP50638J.

[47] D. Fu, K. Liu, T. Tao, K. Lo, C. Cheng, B. Liu, R. Zhang, H.A. Bechtel, J. Wu, Comprehensive study of the metal−insulator transition in pulsed laser deposited epitaxial VO_2 thin films, J. Appl. Phys. 113 (2013) 043707. http://doi.org/10.1063/1.4788804.

[48] M.M. Margoni, S. Mathuri, K. Ramamurthi, R.R. Babu, K. Sethuraman, Investigation on the pure and fluorine doped vanadium oxide thin films deposited by spray pyrolysis method, Thin Solid Films 606 (2016) 51–56. https://doi.org/10.1016/j.tsf.2016.03.035.

[49] D.P. Joseph, C. Venkateswaran, Bandgap engineering in ZnO by doping with $3d$ transition metal ions, J. Phys B-AT MOL OPT 11 (2011) 270540. https://doi.org/10.1155/2011/270540.